

Tadpole type motion of charged dust in the Lagrange problem with planet Jupiter

Christoph Lhotka^{1,2}, Lei Zhou^{2,3}

¹Department of Mathematics, University of Rome Tor Vergata,
Via della Ricerca Scientifica 1, 00133 Roma, Italy,
lhotka@mat.uniroma2.it

²Institute of Astrophysics, University of Vienna,
Türkenschanzstrasse 17, A-1180 Wien, Austria,
christoph.lhotka@univie.ac.at

³School of Astronomy and Space Science, Nanjing University,
163 Xianlin Avenues, 210046 Nanjing, PR China,
leizhou@smail.nju.edu.cn

September 3, 2021

Abstract

We investigate the dynamics of charged dust interacting with the interplanetary magnetic field in a Parker spiral type model and subject to the solar wind and Poynting-Robertson effect in the vicinity of the 1:1 mean motion resonance with planet Jupiter. We estimate the shifts of the location of the minimum libration amplitude solutions close to the location of the L_4 and L_5 points of the classical - gravitational - problem and provide the extension of the 'librational regimes of motion' and the width of the resonance in dependency of the nongravitational parameters related to the dust grain size and surface potential of the particles. Our study is based on numerical simulations in the framework of the spatial, elliptic restricted three-body problem and semi-analytical estimates obtained by averaging of Gauss' planetary equations of motion.

Keywords Charged Dust, Lagrange Problem, Jupiter Trojan, Interplanetary Magnetic Field

1 Introduction

Interplanetary dust particles (IDPs) originate largely from cometary activity and collisions of asteroids in the solar system and form the interplanetary background dust cloud. A better understanding of the dynamics of dust distributions in space will not only help to better understand the current state of our solar

system [Poppe and Lee, 2020, Zhou et al., 2021, Pokorný and Kuchner, 2019], but will also help to design proper spacecraft shielding. Since impacts of dust on spacecraft may strongly influence the quality of spacecraft data (e.g. plasma measurements, see Lhotka et al. [2020]) a better understanding of the distribution and dynamics of IDPs in the vicinity of Jupiter is of particular interest for future space missions (e.g. JUICE and LUCY). In these outer regions, these tiny objects can originate from several sources, including Edgeworth-Kuiper Belt objects, Halley-type comets, Jupiter-family comets, and Oort Cloud comets [Koschny et al., 2019, Poppe, 2016], or the Centaurs [Poppe, 2019]. Additionally, interstellar dust (ISD) has been detected [Krüger et al., 2019, Grün et al., 1993], meaning that some particles from the Local Interstellar Cloud can penetrate the heliosphere and enter the solar system. Research on the dynamics of dust in the solar system in recent years also include the study of the evolution of orbits about comets with arbitrary comae [Moretto and McMahan, 2020], the development of analytical models to investigate the dynamics in phase space [Alessi et al., 2019], and a theoretical study on the dissipative Kepler problem with a family of singular drags [Margheri and Misquero, 2020]. In [Feng and Hou, 2019] the authors study the secular dynamics around small bodies with solar radiation pressure with application to asteroids, the effect of resonances in the Earth space environment has been investigated in [Celletti et al., 2020].

In the present work we focus on the dynamics of charged dust within co-orbital configuration with a planet. In Liu and Schmidt [2018a,b] the authors investigate the orbital evolution of dust released from co-orbital asteroids with planet Jupiter that form an arc, mainly composed of grains in the size range 4-10 microns. The arc is distributed more widely in the azimuthal direction, with two peaks that are azimuthally displaced from the equilibrium position of the pure gravitational problem. The study strongly focuses on the leading Lagrange point L_4 stating that the dust distribution in the vicinity of the region L_5 is similar. However, in Lhotka and Celletti [2015] we already found an asymmetry between the Lagrange points L_4 and L_5 that is caused by the non-gravitational forces, i.e. by the so-called Poynting-Robertson effect, and in Zhou et al. [2021], the effect of asymmetry between the leading and trailing equilibria has also been found in case of planet Venus. However, while our study in Zhou et al. [2021] already included the effect of charge, our study of micron sized dust in the orbit of Jupiter [Lhotka and Celletti, 2015] did not include the effect of the interplanetary magnetic field, like it has already been done in Liu and Schmidt [2018a]. Lorentz force due to the interaction with the magnetic fields cannot be neglected if the charge-to-mass ratios become large (which is true for micron sized particles). The photoelectric effect and charging currents due to space plasmas result in (mostly) positively charged dust grains, with surface potential about 5 Volts [Mann et al., 2014]. For a detailed analysis of different charging mechanisms see also Lhotka et al. [2020]. We notice that the secular effect on charged particles out of resonance has already been investigated in Lhotka et al. [2016], where the authors identify the normal component of the field to trigger secular drift in semi-major axes. In addition, a Parker spiral model of the field results in a

symbol	values	reference
a_1	$a_J = 5.205AU$	(a)
B_0	3nT	Meyer-Vernet [2012]
η	1/3	Klačka [2014]
i_0	7.15°	Beck and Giles [2005]
m_0	M_\odot	(a)
m_1	$m_J = 0.001M_\odot$	(a)
r_0	1AU	Meyer-Vernet [2012]
Ω_0	73.5°	Beck and Giles [2005]
Ω_s^{-1}	24.47d	Meyer-Vernet [2012]
Q	1	Beauge and Ferraz-Mello [1994]
ρ	$2.8g/cm^3$	Beauge and Ferraz-Mello [1994]
u_{sw}	400km/s	Meyer-Vernet [2012]

Table 1: Parameters, (a) taken from <https://nssdc.gsfc.nasa.gov/planetary/factsheet/>.

normal component in the Lorentz force that will strongly affect the inclination of the orbital planes. This is also true for charged particles in mean motion resonance with planet Jupiter. As it has been shown in Lhotka and Galeş [2019] the interaction with the interplanetary magnetic field destabilizes the orbits of charged dust grains also in outer mean motion resonance with the planet.

In the present study we aim to complement these previous results. We study the dynamics of micron sized dust and co-orbital with planet Jupiter, and i) include the role of charge together with the effect of the interplanetary magnetic field and ii) also perform the analysis of dust grain motion close to the trailing Lagrange point L_5 . In addition, we provide a thorough analysis of the extent of the resonant regime of motion in dependency of the system parameters, i.e. charge-to-mass ratio and size-to-mass ratio, and provide information about typical times of temporary capture in tadpole and also co-orbital type of motions.

This work is organized as follows. In Section 2 we state the notation and dynamical problem that we are going to use in our study. The analysis of the numerical simulation data is given in Section 3. The discussion of certain aspects of the dynamics based on Gauss' equations of motion is provided in Section 4. The summary of the results and conclusions can be found in Section 5.

2 Notation and set-up

The orbital evolution of a charged dust grain is determined by the equation of motion

$$\ddot{\vec{r}} + \mu \frac{\vec{r}}{r^3} = \vec{F} . \quad (1)$$

Here, \vec{r} is the position of the dust grain in a heliocentric coordinate frame with $r = |\vec{r}|$, and $\mu = Gm_0$ with gravitational constant G and mass of the sun m_0 . In absence of perturbing force \vec{F} (per unit mass) the particle is assumed to move on a Kepler orbit with constant orbital elements a (semi-major axis), e (eccentricity), i (inclination), ω (perihelion argument), Ω (ascending node longitude), mean anomaly M , and mean motion n . Let \vec{F} be decomposed into $\vec{F} = \vec{F}_0 + \dots + \vec{F}_3$ with:

$$\begin{aligned}
\vec{F}_0 &= -\beta\mu\frac{\vec{r}}{r^3} \\
\vec{F}_1 &= -\nabla\mu_1\left(\frac{\vec{r}_1\cdot\vec{r}}{r_1^3} - \frac{1}{\Delta} - \frac{1}{r}\right) \\
\vec{F}_2 &= -\frac{\mu\beta}{r^2}\left(1 + \frac{\eta}{Q}\right)\left(\frac{(\dot{\vec{r}}\cdot\vec{g}_r)\vec{g}_r + \dot{\vec{r}}}{c}\right), \\
\vec{F}_3 &= \gamma\left(\dot{\vec{r}} - \vec{u}_{sw}\right) \times \vec{B}.
\end{aligned} \tag{2}$$

Here, \vec{F}_0 is due to solar radiation pressure, \vec{F}_1 is the gravitational force from planet Jupiter, \vec{F}_2 is stemming from the so-called Poynting-Robertson effect and solar wind drag [Klačka et al., 2012, Klačka, 2014], and \vec{F}_3 is the Lorentz force term stemming from the interaction of the charged particle with the interplanetary magnetic field [Lhotka and Narita, 2019]. We denote by $m = 4\pi/3\rho R^3$ the mass of a spherical dust grain of radius R with density ρ , and by $q = 4\pi\varepsilon_0UR$ its charge for given surface potential charge U and dielectric constant ε_0 . The equations (2) enter the remaining quantities (in the order of appearance): the parameter $\beta \propto R^{-1}$, which is the ratio between the magnitudes of solar radiation pressure and gravitational force due to the sun:

$$\beta = \frac{SQ\pi R^2}{c} \left(\frac{r_0}{r}\right)^{-2} / \frac{\mu m}{r^2}$$

(we notice that both forces are proportional to the inverse square of the distance from the sun). Setting the solar flux constant $S = 1360.8\text{kg}s^{-3}$ at reference distance $r_0 = 1AU$, the dimensionless efficiency factor $Q = 1$, speed of light $c = 299792458\text{m/s}$, $\mu = 1.327 \times 10^{20}\text{m}^3\text{s}^{-2}$, and $m = 11.7286\text{gcm}^{-3}$, we find $\beta = 0.205/R$, with R given in micro-meters. The additional quantities are the gravitational mass of Jupiter $\mu_1 = Gm_1$, the heliocentric position vector for planet Jupiter, \vec{r}_1 , the distance between Jupiter and the dust grain $\Delta = \|\vec{r} - \vec{r}_1\|$, the solar wind efficiency factor η , $\vec{g}_r = \vec{r}/r$, the charge-to-mass ratio $\gamma \propto UR^{-2}$, the solar wind speed $\vec{u}_{sw} = u_{sw}\vec{g}_r$, and the interplanetary magnetic field vector \vec{B} . Our main focus lies in the role of parameters β , γ related to the physical parameters size and charge. Assuming spherical particles, and using the actual values for the various parameters entering (2) that are given in Tab. 1, we find:

$$\beta = 0.205/R \quad \gamma = 0.0094U/R^2, \tag{3}$$

with R given in micro-meters and U given in Volts. We are left to specify the form of the interplanetary magnetic field vector:

$$\vec{B} = \frac{B_0 r_0^2}{r^2} \left(\frac{\vec{r}}{r} - \frac{\Omega_s}{u_{sw}} \vec{g}_z \times \vec{r} \right) \tanh \left(\alpha \frac{\vec{r} \cdot \vec{g}_z}{r} \right), \quad (4)$$

with background magnetic field strength B_0 defined at reference distance r_0 , and solar rotation rate Ω_s . The form of the \vec{B} field enters the parameter α to model the sign change when crossing the equatorial plane of the sun¹, and the unit vector along magnetic north \vec{g}_z that is related to the heliocentric reference frame $\{\vec{g}_x, \vec{g}_y, \vec{g}_z\}$ by

$$\vec{g}_z = \sin(i_0) [\sin(\Omega_0) \vec{g}_x - \cos(\Omega_0) \vec{g}_y] + \cos(i_0) \vec{g}_z.$$

Here, i_0 denotes the inclination between the rotation axis of the sun and the ecliptic pole and Ω_0 is the angle between the direction of the vernal equinox and the line of nodes between the equatorial and ecliptic planes, respectively. Please see Fig. 1 for visualization of the various reference frames. The actual parameters used in our study are summarized in Tab. 1, for further details on the model, see Lhotka and Galeš [2019].

3 Numerical study and results

We start with a short phenomenological description of the phase space in dependency of the system parameters. First, we integrate (1) and choosing 60 initial conditions within the orbital plane of Jupiter with $\sigma(0)$ (where $\sigma = \lambda - \lambda_J$ and mean orbital longitudes λ and λ_J) ranging from 0 to 360° and setting $\omega(0)$, $\Omega(0)$ equal $\omega_J \pm 60^\circ$, Ω_J as well as $a(0)$, $e(0)$ equal a_J , e_J . We stop the integration of the individual orbits at time $t = 5000$ yr or at close encounter with planet Jupiter. The simulation time has been fixed to ensure a complete covering of the phase space. We notice, that erosion timescales of dust in space may be much shorter, and strongly depend on the space environment and the chemical composition of the dust grain [see, e.g. Spahn et al., 2019]. The projection of the orbits to the plane (σ, a) for $\beta = 0$ and $\gamma = 0$ is shown in Fig. 2. In the classical problem we clearly see the location of the tadpole and horseshoe type regimes of motion. The centers of librational kinds of motions are located at $\sigma = \sigma_4 = 60^\circ$ and $\sigma = \sigma_5 = 300^\circ$ - that define the positions of the Lagrange points L_4 and L_5 , respectively. The saddle, denoted by L_3 is situated at $\sigma = \sigma_3 = 180^\circ$ at the crossing of the separatrix that divides librational and rotational motion close to resonance. We notice that for the center orbits $e(t) \simeq e(0)$, $\omega(t) \simeq \omega(0)$, $\forall t$, and that the uncharged dust grains stay within the orbital plane of Jupiter during the whole integration time (not shown here). For the same set of parameters and initial conditions as before we integrate (1), but with $\sigma(0) = \pm 60^\circ$ and taking the values for $\Delta\omega(0) \in (-180^\circ, 180^\circ)$, with $\Delta\omega = \omega - \omega_J$. We do not show

¹We assume that the magnetic dipole axis and the rotation axis of the sun are aligned and that the equatorial plane of the sun therefore coincides with the zero current sheet.

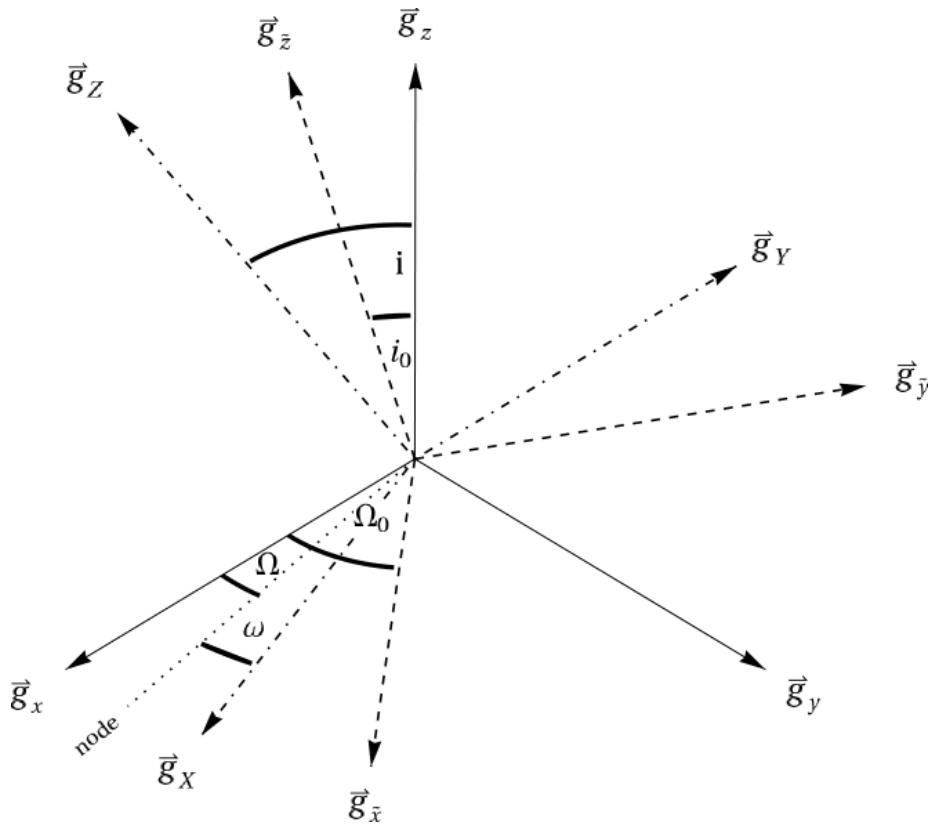


Figure 1: Geometry of the problem: ecliptic frame (x, y, z) , equatorial frame $(\tilde{x}, \tilde{y}, \tilde{z})$, orbital frame (X, Y, Z) . The nodal line refers to the intersection between the ecliptic and orbital planes. For the definitions of the angles, see text.

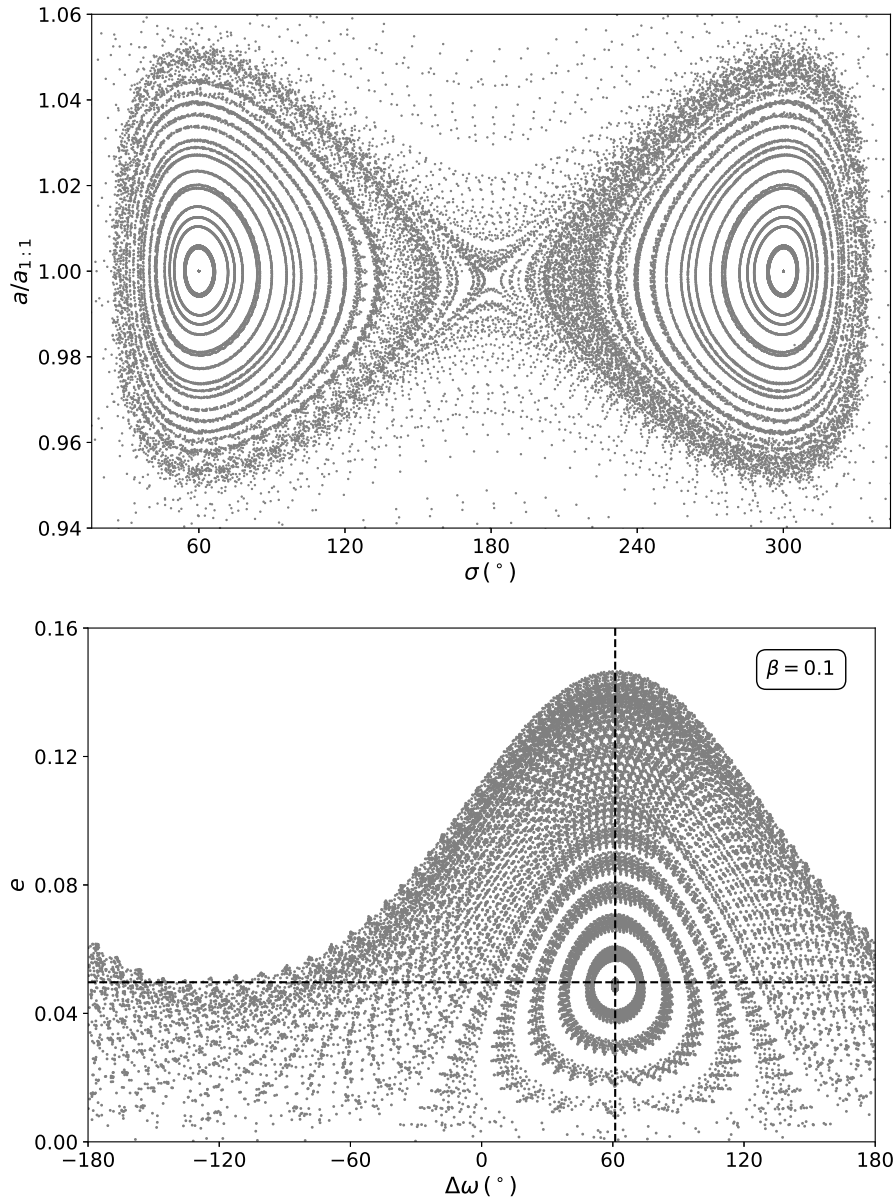


Figure 2: Top: phase portrait (section σ vs. $a/a_{1:1}$) for value of parameter $\beta = 0$, $\gamma = 0$. Bottom: projection ($\Delta\omega = \omega - \omega_J$ vs. e) for $\beta = 0.1$ and uncharged dust particles in the vicinity of L_5 .

the results for the classical problem ($\beta = 0$) here, but report that oscillatory behaviour takes place close to $\Delta\omega = \pm 60^\circ$, $e = e_J$, with increasing libration amplitudes for larger values of $e(0)$ as expected and already shown by previous studies.

For $\beta \neq 0$ the perturbations due to solar radiation pressure and the combined Poynting-Robertson effect and solar wind drag lead to additional distortions of the orbits. We provide the results in the $(\Delta\omega, e)$ -plane at the bottom of Fig. 2. We notice that the orbits are actually not following invariant curves, but rather resemble the projection of a $6D$ phase space spanned by the Kepler elements $(a, e, i, \omega, \Omega, M)$ to a suitable choice of variables in $2D$. We also integrate (1) for 60 initial conditions up to integration time 5000 yr and project the orbits to the plane (σ, a) . The results are shown at the top of Fig. 3 and should be compared to Fig. 2. While the orbits for the case $\beta = 0$ follow the geometry of the classical CRTBP (Circular Restricted Three-Body Problem) with narrow widths close to the libration centers, the majority of the orbits at the top in Fig. 3 fill up the full tadpole regime of motions. The asymmetry in the shifts from 60° , -60° between L_4 , L_5 is clearly present in the plane (σ, a) . While the offset from the location of L_4 from 60° is about 7.71° for $\beta = 0.5$ the shift is only about 5.52° from the location of L_5 at 300° for $\beta = 0$. As it can be seen by the vertical dashed lines in Fig. 3 the shift from 180° (the location of L_3 for $\beta = 0$) is about 2.66° at $\beta = 0.5$. This asymmetry in phase space due to the different response of micron-sized particles between L_4 and L_5 will be addressed in full detail later in this section.

The role of charge on the dynamics is three-fold: i) first, the additional perturbations lead to even stronger distortions when projected to the plane (σ, a) - see bottom of Fig. 3, where 30 orbits with initial $\sigma(0)$ from 0 to 360° are integrated for 5000 yr; ii) the interaction with the interplanetary magnetic field prevents the charged dust particles to perform regular, oscillatory type of motions in the $(\Delta\omega, e)$ -plane (but still close to the centers, not shown here); iii) finally, Lorentz force acts transversal to the orbital plane of Jupiter and leads to excursions of the dust grains to high ecliptic latitudes that cannot be seen in the uncharged problem, see lower left of Fig. 4, where we show three individual orbits starting with the same initial conditions, but different charge-to-mass ratios corresponding to $0V$, $5V$, and $10V$ surface potential, respectively.

The comparison of the pure gravitational problem together with the uncharged one including solar radiation pressure and Poynting-Robertson effect with the charged problem, already demonstrates the role of β and γ on the topology of the phase space. Next, we aim to quantify the dependency on these system parameters of 1) the location of the orbit with minimum libration amplitudes (that corresponds to an equilibrium in the classical problem), 2) the effect of β and γ on the libration width of the 1:1MMR, and 3) their role on the time of temporary capture close to resonance. To start with 1) we require a robust and suitable numerical tool to be defined in the next section.

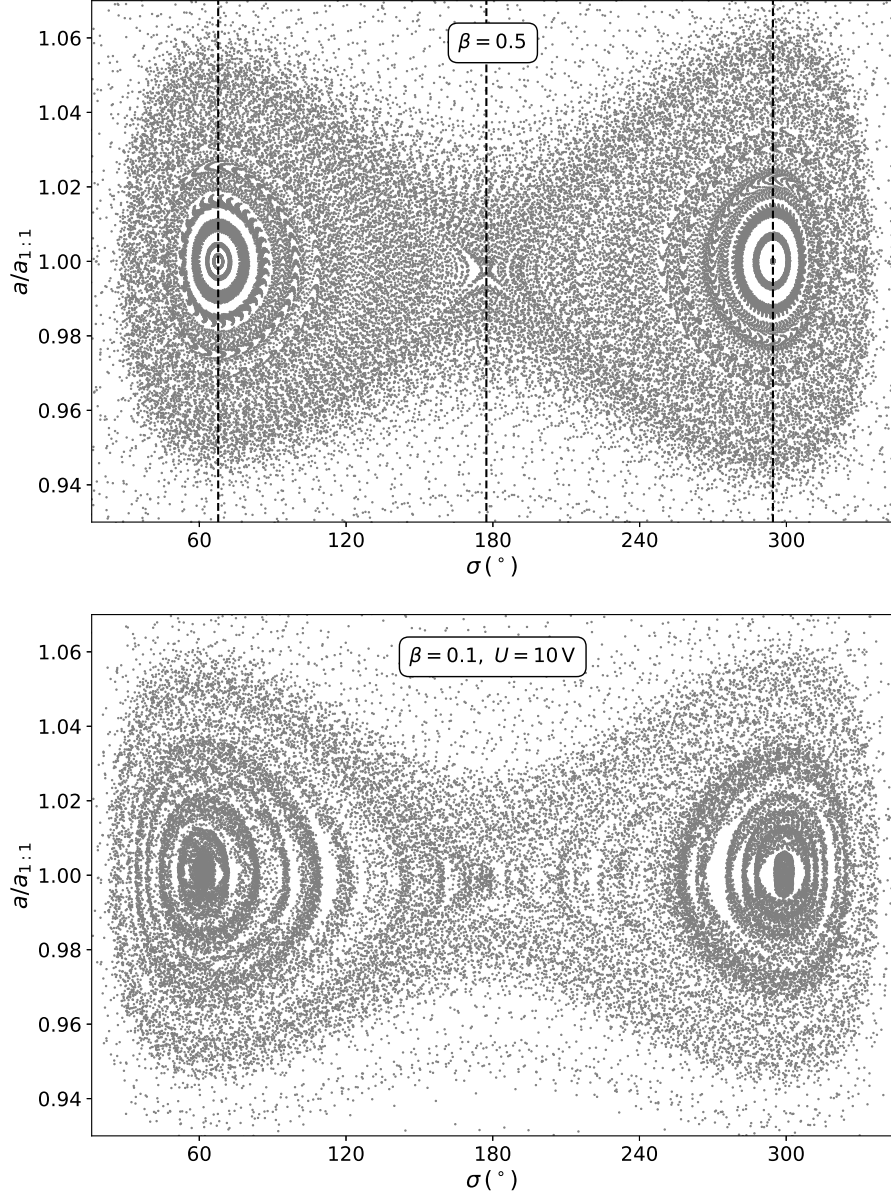


Figure 3: Top: phase portrait (section σ vs. $a/a_{1:1}$) for value of parameter $\beta = 0.5$, $\gamma = 0$. The resonant angles of the Lagrangian points L_4 , L_3 and L_5 , shown by vertical lines, are 67.71° , 177.34° and 294.48° , respectively. Bottom: same initial conditions, but with $\beta = 0.1$ and $10V$ surface potential.

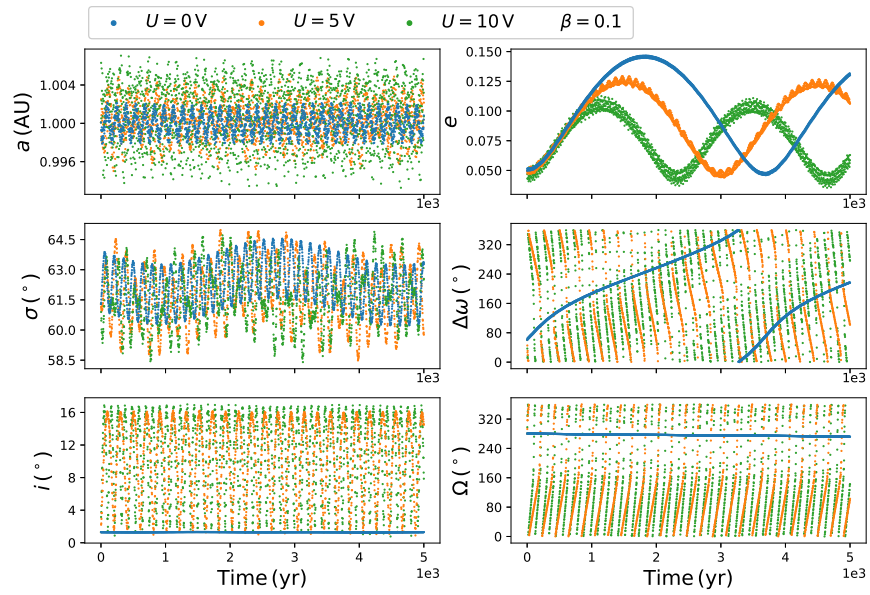


Figure 4: Orbital evolution of particles starting from the location of L_4 (but $\Omega(0) = \Omega_J + 180^\circ$) in the uncharged problem with $\beta = 0.1$. The blue curve indicates the uncharged model while the orange and green curves indicate the orbital evolution of charged particles.

3.1 Minimum libration amplitude solutions

Let $w_T = w_T(X_j, \vec{X}_0; \beta; \gamma)$ be the maximum libration amplitude of the j -th component $X_j = X_j(t)$ of vector $\vec{X} = \vec{X}(t)$ during the integration time $0 \leq t \leq T$, starting with the initial condition $\vec{X}_0 = (a_0, e_0, i_0, \Delta\omega_0, \Omega_0, \sigma_0)$, and for fixed values of the parameters β, γ . Let $\vec{X}^* = (a^*, e^*, i^*, \Delta\omega^*, \Omega^*, \sigma^*)$ be the initial condition that defines the location of L_4 with $a^* = a_J, e^* = e_J, i^* = i_J, \Delta\omega^* = 60^\circ, \Omega^* = \Omega_J$, and $\sigma^* = 60^\circ$ (or $\Delta\omega^* = 300^\circ, \sigma^* = 300^\circ$ in case of L_5). For vanishing values of the parameters β, γ and in exact steady-state configuration we have $w_T(X_j, \vec{X}^*, 0, 0) \simeq 0$ for all j , while for non-zero β, γ we generally find $w_T(X_j, \vec{X}^*, \beta, \gamma) = \delta_j$ with $\delta_j > 0$ and $j = 1, \dots, 6$. To obtain a minimum libration amplitude solution we minimize w_T with respect to X_j starting in the vicinity of \vec{X}^* , say $\vec{X}_{\varepsilon_j}^*$ with $X_j(0) = X_j^* \pm \varepsilon_j$ and positive ε_j :

$$\delta_j = \min_{X_j^* - \varepsilon_j \leq X_j \leq X_j^* + \varepsilon_j} w_T(X_j, \vec{X}_{\varepsilon_j}^*, \beta, \gamma), \quad j = 1, \dots, 6. \quad (5)$$

Our aim is to minimize all δ_j with $j = 1 \dots 6$ for fixed pair (β, γ) . We start with the case $\beta > 0$ and $\gamma = 0$. Since solar wind drag and Poynting-Robertson effect does not influence ascending node longitude and inclination of the orbital plane we keep $X_5 = \Omega^*, X_3 = i^*$ fixed. Taking into account that the libration amplitudes are strongly coupled in pairs (a, σ) and $(e, \Delta\omega)$ - see phase portraits in the previous section - we minimize (5) in an iterative way as follows.

Let $\vec{X}_{\varepsilon_j, r}^*$ be the initial condition during the r -th iteration process with $\vec{X}_{\varepsilon_j, 0}^* = \vec{X}_{\varepsilon_j}^*$. We start with a set of initial conditions on a grid in (a, σ) using $a(0) = a_J(1 - \beta)^{1/3} \pm \varepsilon_1$ and $\sigma(0) = \sigma^* + \varepsilon_6$ with $\varepsilon_1 > 0$ and $0 \leq \varepsilon_6 \leq 120^\circ$ and integrate (1) up to time T . Here, the choice for $a(0)$ is motivated by the estimate that follows. Kepler's 3rd law for planet Jupiter takes the form:

$$n_J^2 a_J^3 = \mu,$$

while the law for the dust particle, including radiation pressure, becomes:

$$n^2 a^3 = \mu(1 - \beta).$$

Eliminating μ in above equations we find the relation

$$n^2 a^3 = n_J^2 a_J^3 (1 - \beta),$$

and taking into account $n_J = n$, in presence of a 1:1 MMR, we finally arrive at

$$a = a_J(1 - \beta)^{1/3}.$$

Next, we choose, out of the set of orbits, the initial condition with the minimum libration amplitude solution and identify it with $\vec{X}_{\varepsilon_{1,6}, r=1}^*$ and repeat the above iteration step with smaller $\varepsilon_1, \varepsilon_6$ to obtain $\vec{X}_{\varepsilon_{1,6}, r+1}^*$. The iteration

stops if no significant decrease in libration amplitude can be found anymore when decreasing $\varepsilon_1, \varepsilon_6$. Let a^{**}, σ^{**} be the initial condition of the minimum libration amplitude solution at the final iteration step R . As it turns out the choice $a(0) = a^{**} = a_J(1-\beta)^{1/3}$ is the correct choice for the minimum libration amplitude solution for $\gamma = 0$ while $\sigma(0) = \sigma^{**}$ is shifted from the equilibrium of the classical problem with increasing value of β . Next, we repeat above procedure by fixing $a(0) = a^{**}, \sigma(0) = \sigma^{**}$, and minimizing w_T with respect to $X_2(0) = e(0), X_4(0) = \Delta\omega(0)$ on a grid $(e, \Delta\omega)$ and using $\varepsilon_2, \varepsilon_4$. We start by integrating (1) with initial conditions $e(0) = e_J \pm \varepsilon_2$ and $\Delta\omega(0) = \pm 60 \pm \varepsilon_4$ with $\varepsilon_2, \varepsilon_4 > 0$, and again identify the initial condition that results in the minimum libration amplitude solution with $\vec{X}_{\varepsilon_2, 4=0, r=1}$. We repeat the iterative procedure to obtain e^{**} and $\Delta\omega^{**}$ at iteration step $r = R$. As it turns out, for the case $\gamma = 0$, w_T is minimal for the choice $e(0) = e^{**} = e_J$, while $\Delta\omega^{**}$ gets shifted from the equilibria defined for $\beta = 0$ with increasing values of β like in the case for σ .

The whole process is done for different values of β and for starting values close to L_4 and also L_5 . Let us denote by $a_k, e_k, i_k, \Delta\omega_k, \Omega_k$, and σ_k the final optimal values that minimize w_T , with $k = 4$ in the vicinity of L_4 and $k = 5$ close to L_5 for fixed value of β .

The results for variables σ_k and $\Delta\omega_k$ are shown in Fig. 5. On the top we report the value of σ (by squares) with the minimum of the maximum libration amplitude during the integration time for given values of the parameter β in the vicinity of L_4 (blue) and close to L_5 (orange). The lines are obtained from a theory based on the circular restricted three-body problem including solar radiation pressure and the Poynting-Robertson effect [see, e.g. Schuerman, 1980, Zhou et al., 2021] and confirm the values obtained by minimizing (5). At the bottom of Fig. 5 we report the results for $\Delta\omega_k$ close to L_4 (blue) and L_5 (orange), both obtained by minimizing (5). In both figures we clearly see the shift of the minimum libration amplitude solutions in dependency of parameter β up to 1.5 degrees at $\beta = 0.1$. The two panels in Fig. 5 also reveal an asymmetry between the Lagrange points L_4 and L_5 . While the shift in σ from 60° is more prominent for solutions close to L_4 , in comparison to the shift from -60° (close to L_5), the situation is reversed in the shift of $\Delta\omega$. The findings confirm the results, already obtained in Lhotka and Celletti [2015], where the authors use a semi-analytical approach in the framework of the restricted three-body problem (circular, elliptic, and spatial) that is based on averaged equations of motions.

Next, we repeat by minimizing (5) wrt. $a(0), e(0), \Delta\omega(0), \sigma(0)$ for $\gamma > 0$, i.e. for dust grain surface potentials equal 5 and 10 Volts, in the same way as for the case $\gamma = 0$. We find a strong influence of charge on the dynamics as demonstrated by the example shown in Fig. 6. The figure shows the libration amplitudes $\Delta\sigma$ on a grid of initial conditions $\sigma(0) \times \delta a(0)$, with $\delta a = a - a_{1:1}$, for two different values of β and 5 Volts surface charge in the vicinity of L_4 . The location of the minimum libration amplitude solutions in the uncharged case are given by black-dashed lines and we clearly see that in the presence

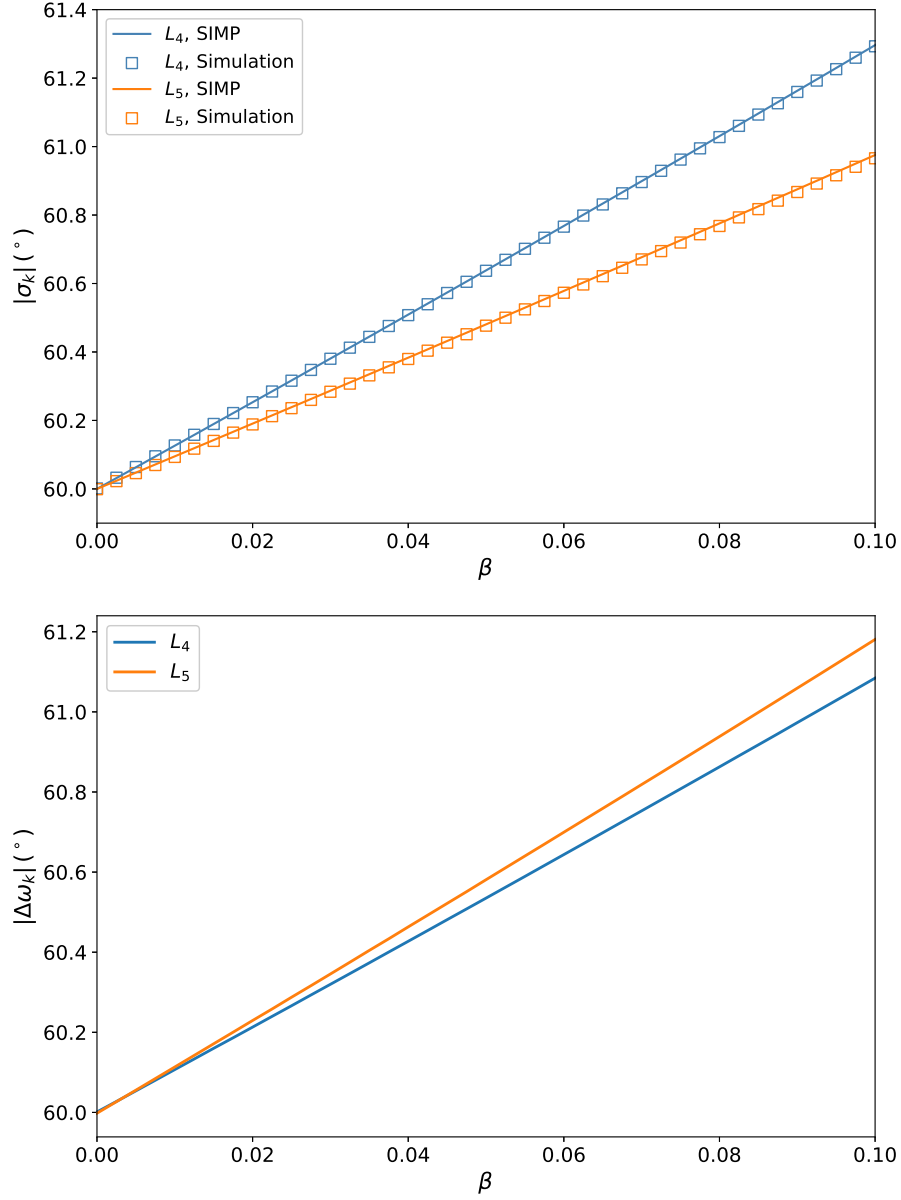


Figure 5: Dependency of minimum libration amplitude in σ_k (top) and $\Delta\omega_k$ (bottom) with $k = 4, 5$ corresponding to L_k on parameter β (and $\beta = 0$ indicated by black-dashed line). We note that the y -axis is the absolute value of σ_k and $\Delta\omega_k$ in the range of $(-180^\circ, 180^\circ)$.

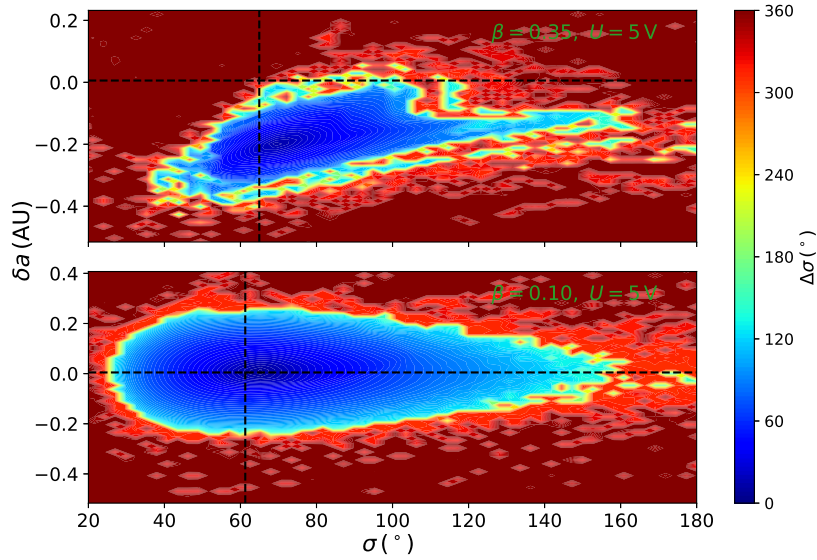


Figure 6: Libration amplitudes ($\Delta\sigma$) on the (σ, a) plane in the charged problem ($U = 5$ V) with $\beta = 0.1$ (bottom) and $\beta = 0.35$ (top). The dashed lines indicate (σ_k, a_k) in the uncharged problem for the corresponding value of β . We note the y -axis is the deviation from the nominal value $a_{1:1}$.

of charge this location (dark-blue) gets shifted towards smaller values in semi-major axis a and larger values in σ . The effect becomes stronger for larger values of β (allowing larger values in γ for same surface potential charge): while the deviation in δa is smaller and symmetric with respect to the symmetry line $\delta a = 0$ it becomes larger and asymmetric in the case $\beta = 0.35$. We also notice that with increasing β the region of librational motion shrinks. Solar wind, Poynting-Robertson effect as well as the interplanetary magnetic field strongly affect the dynamics. In the following we report the location and parameters for the minimized solution with respect to librational amplitudes, i.e. the location of the darkest blue region in simulations of the type as shown in Fig. 6, in dependency of the system parameters.

We summarize our study for different values of β in case of dust grain surface potentials equal 5 and 10 Volts in Fig. 7, 8, where the results are given relative to the solution of minimum libration amplitude of the uncharged case. At the top of Fig. 7 we report the shift δa_4 in blue and relative to a_4 due to $\gamma > 0$ for 5 Volts. With increasing value of β we find a negative shift that becomes larger in magnitude and reaching 0.01 AU for $\beta = 0.1$. In Fig. 7 we also report the shift $\delta\sigma_4$ in orange and relative to σ_4 , that again becomes larger with increasing values of β (and γ) reaching several degrees of offset at $\beta = 0.1$. The results in $\delta a_5, \delta\sigma_5$ are shown at the bottom of Fig. 7 with comparable values in δa_5 ($\delta\sigma_5$)

in comparison with δa_4 ($\delta \sigma_4$). We notice the presence of spikes close to $\gamma \simeq 0.01$ in both panels that are also present for different surface potential of the dust grains (see, Fig. 8 in case of 10Volts). We notice that for larger values of the surface potential these spike like structure is shifted towards smaller values in β but still remains close to the value $\gamma \simeq 0.01$.

Where does it come from? A series of simulations with various initial conditions and parameters suggests that the spikes are the result of a commensurability between the precession rate $\dot{\Omega}$ of the ascending node longitude and the period in libration of the resonant angle σ . As demonstrated in Fig. 9 the variations in amplitude of the angle σ are greatly enhanced for the case $U = 5V$ (in orange), where the fundamental period in Ω (and i) is about the same as for the resonant argument itself. On the contrary, the amplitude variations stay small during the whole integration period in the uncharged case $U = 0V$, and for the case $U = 10V$. We remark that the period in Ω is inversely proportional to the parameter γ , or Γ - as it has been shown in Lhotka and Galet [2019]. As a result, for $U = 10V$, the period of Ω and i is only half of the value for $U = 5V$, as it is confirmed also by the bottom two panels of Fig. 9. Since the libration period of σ stays the same for different values of β , the values of the parameter γ which determine the period of Ω could finally determine the locations of the spike at the same value of γ , although the corresponding values of β are different, since $\beta \propto 1/R$ while $\gamma \propto U/R^2$ - see also (3).

The results for minimum libration amplitude solutions concerning the variables $\Delta\omega_k$ and e_k are reported in Fig. 10. An important effect of charge, that is clearly visible, is the change of e_k wrt. to β (γ) that cannot be seen in the uncharged problem, subject to solar wind and the Poynting-Robertson effect alone. While for $\gamma = 0$ we have $e_k = e_J \simeq 0.050$ we get $e_k \simeq 0.040$ for $\beta = 0.1$ (top of Fig. 10) and a minimum in $e_k = 0.045$ close to L_5 (at the bottom of the figure). The shift of $\Delta\omega_k$ for $\gamma > 0$ also turns out to be more prominent in comparison to the shifts in σ_k . As we can see in Fig. 8 the maximum shift is about 2° in $\Delta\omega_4$ (top) and about 2° in $\Delta\omega_5$ (bottom).

3.2 Resonance width and time of temporary capture

Once the initial conditions for the minimum libration amplitude solutions have been found we are interested in the extend of the librational regime of motions around L_4 and in the vicinity of L_5 in dependency of parameters β and γ . To estimate the ‘libration widths’ we start by integrating (1) using the initial conditions from the previous study and increase $a(0) = a^* + \delta a$ with $\sigma(0) = \sigma_k$ (with $k = 4$ close to L_4 and $k = 5$ in case of L_5) until i) the maximum value of the resonant argument $\sigma(t)$ goes beyond σ_5 (thus $\sigma(t) > \sigma_5$) in case of orbits originating from L_4 or ii) we find $\sigma(t) < \sigma_4$ for integrations starting around L_5 . We report the size of the value δa at which the crossing of the librational regime takes place in Fig. 11 for different values of the parameter β and using $\gamma = 0$. We clearly see that due to the additional perturbations δa decreases with increasing value of β with a steeper slope in case of orbits originating from L_4 (blue crosses) in comparison to L_5 (orange circles). Thus, solar wind and

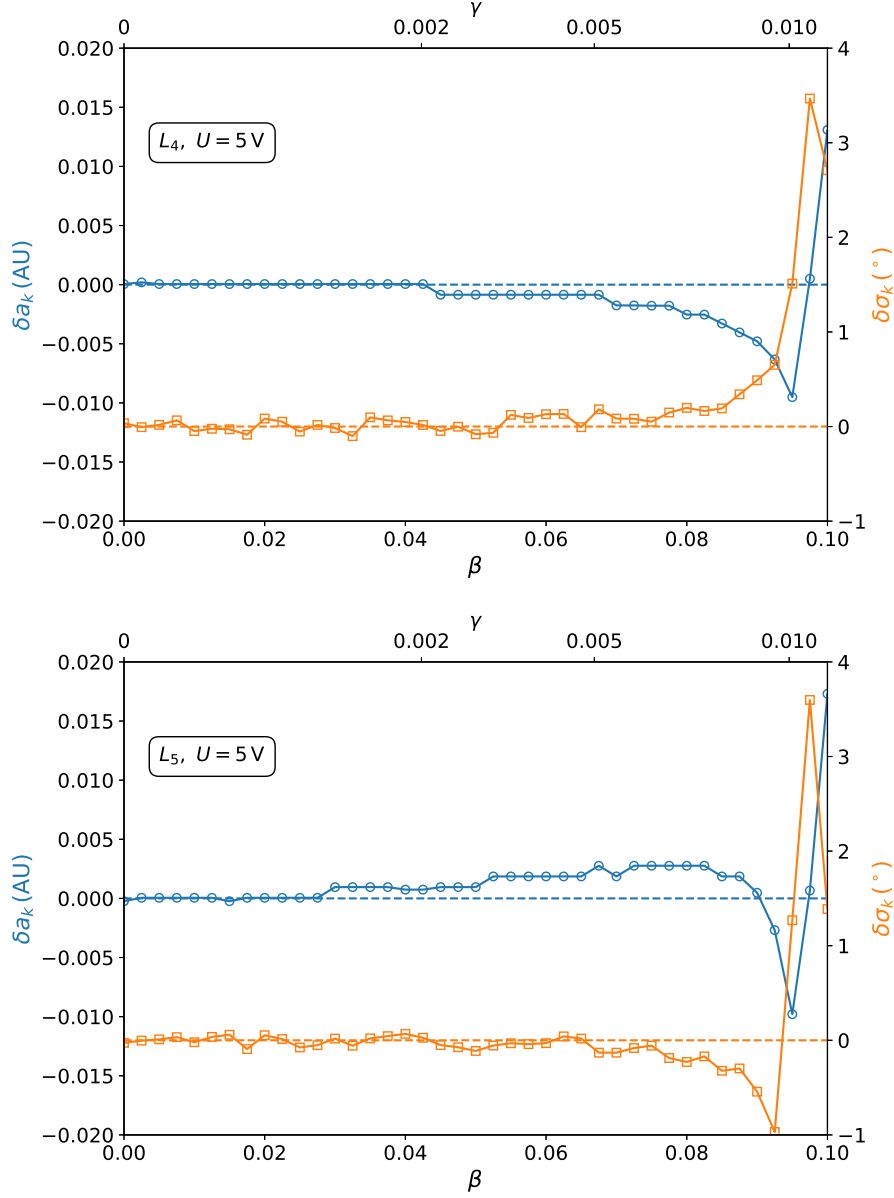


Figure 7: Deviation from minimum libration amplitudes of uncharged problem for dust grain potential surface charge of 5 Volts in semi-major axes δa_k and resonant angles $\delta \sigma_k$ (with $k = 4$ in the vicinity of L_4 - top and $k = 5$ close to L_5 - bottom). The cases with $V = 0$ Volts are shown by dashed lines.

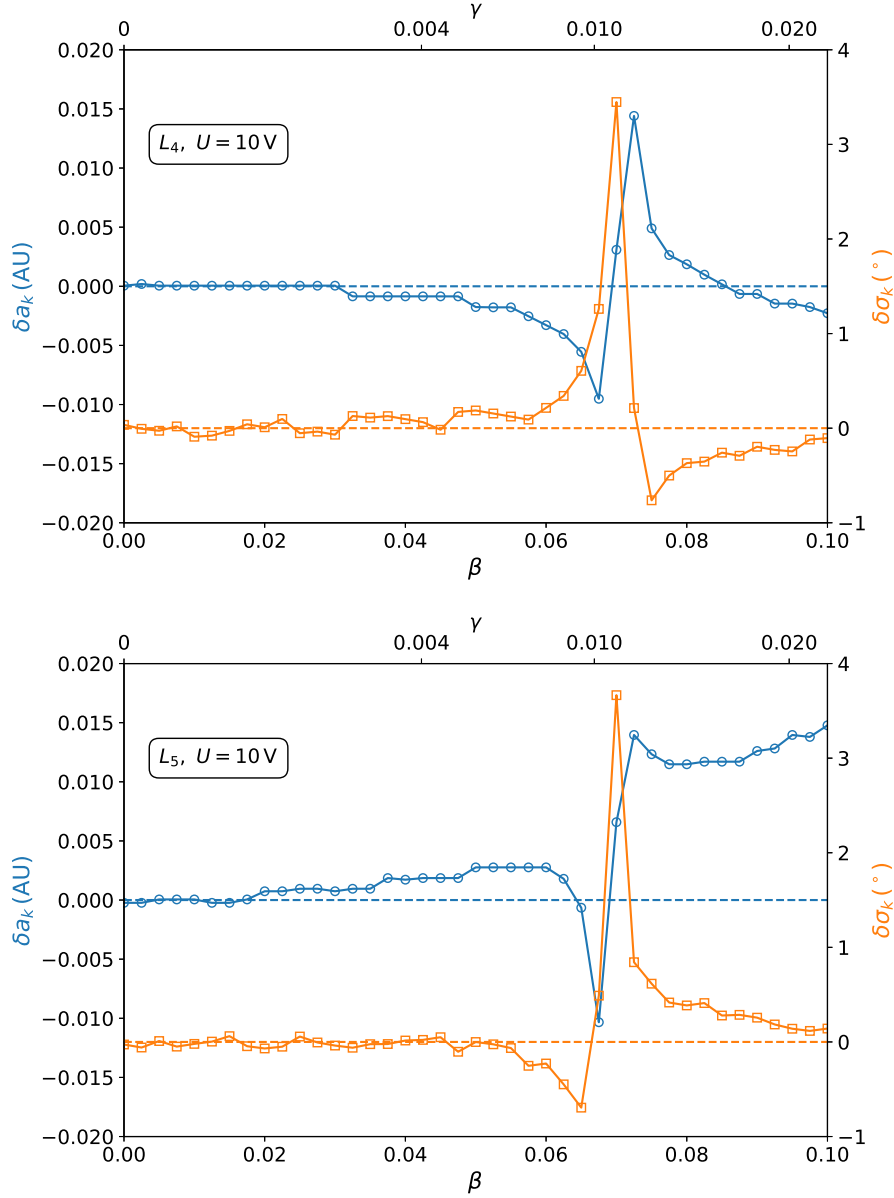


Figure 8: Deviation from minimum libration amplitudes of uncharged problem for dust grain potential surface charge of 10 Volts in semi-major axes δa_k and resonant angles $\delta \sigma_k$ (with $k = 4$ in the vicinity of L_4 - top and $k = 5$ close to L_5 - bottom). The cases with $V = 0$ Volts are shown by dashed lines. Compare with Fig. 7.

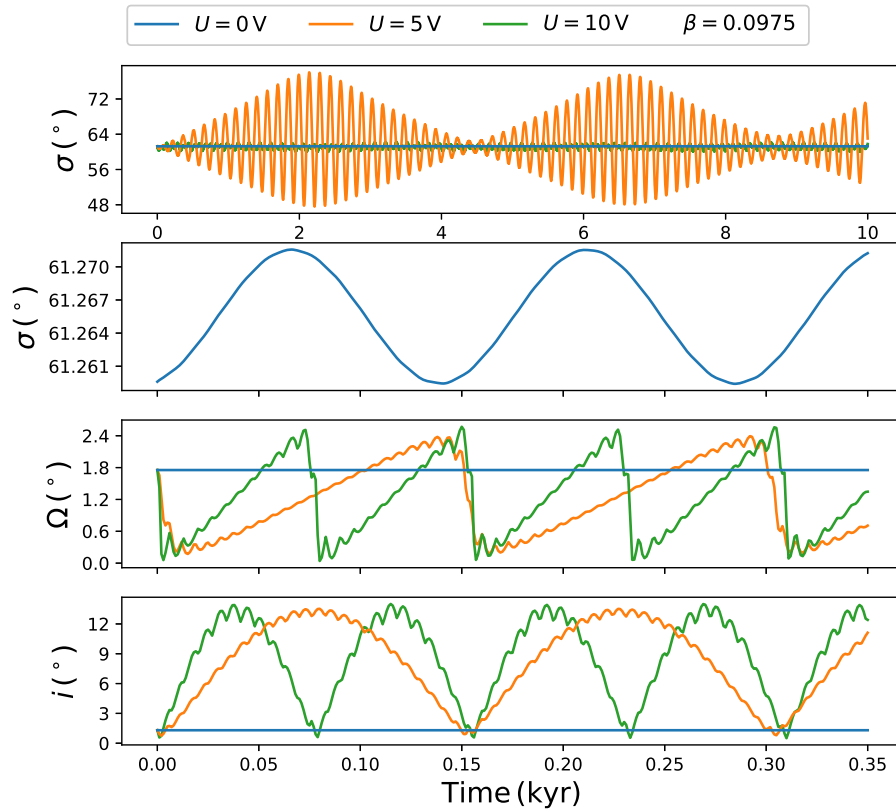


Figure 9: Occurrence of the spike in Fig. 7 for $\beta \simeq 0.1$, $\gamma \simeq 0.01$ (orange with $U = 5V$). Enhancement of amplitude variations of resonant argument, resonant argument in uncharged case (blue with $U = 0V$), evolution of ascending node longitude, and inclination (from top to bottom). For $U = 10V$ (green) the spike does not show up at $\beta \simeq 0.01$.

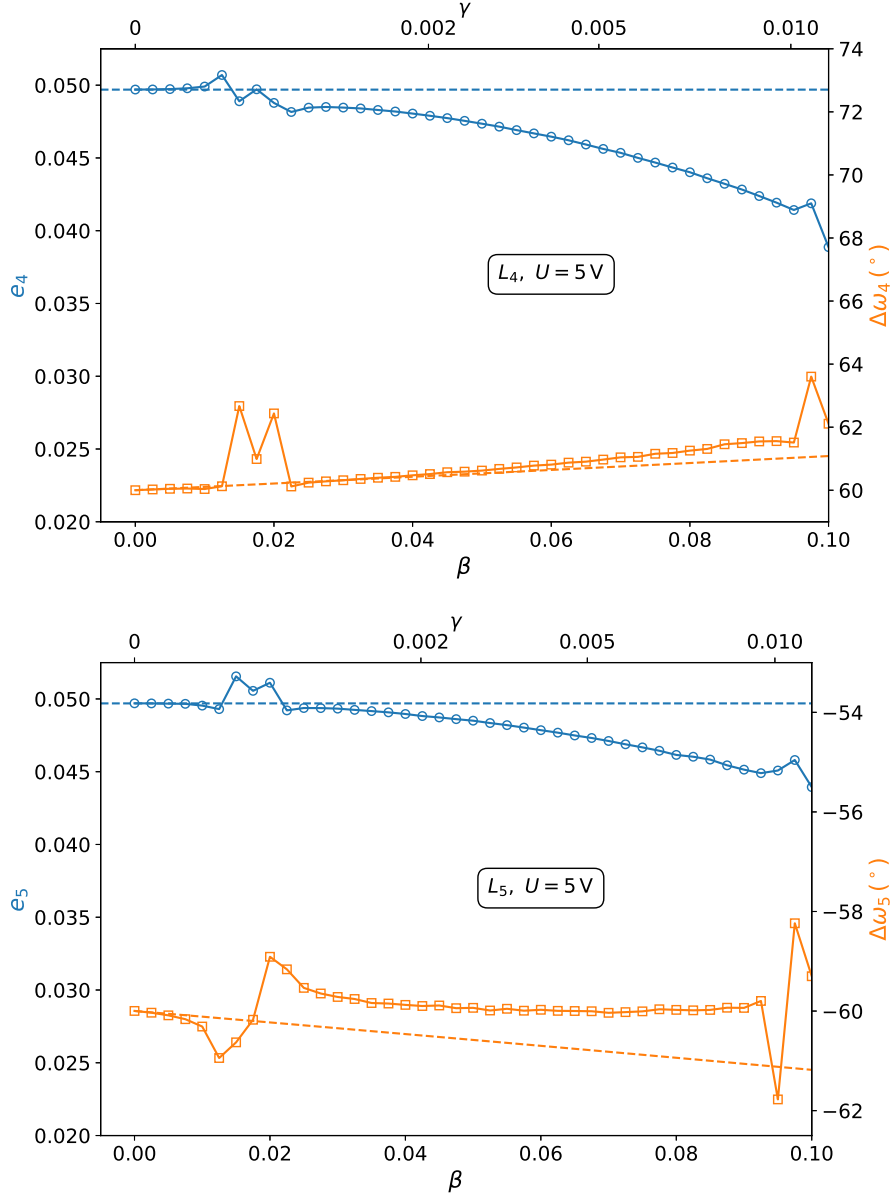


Figure 10: Dependency of minimum libration amplitude in e_k (blue) and $\Delta\omega_k$ (orange) in the vicinity of L_k (with $k = 4$ on top and $k = 5$ at the bottom) on parameter β and γ (the cases $\gamma = 0$ are indicated by dashed lines) and dust grain surface potential 5 Volts.

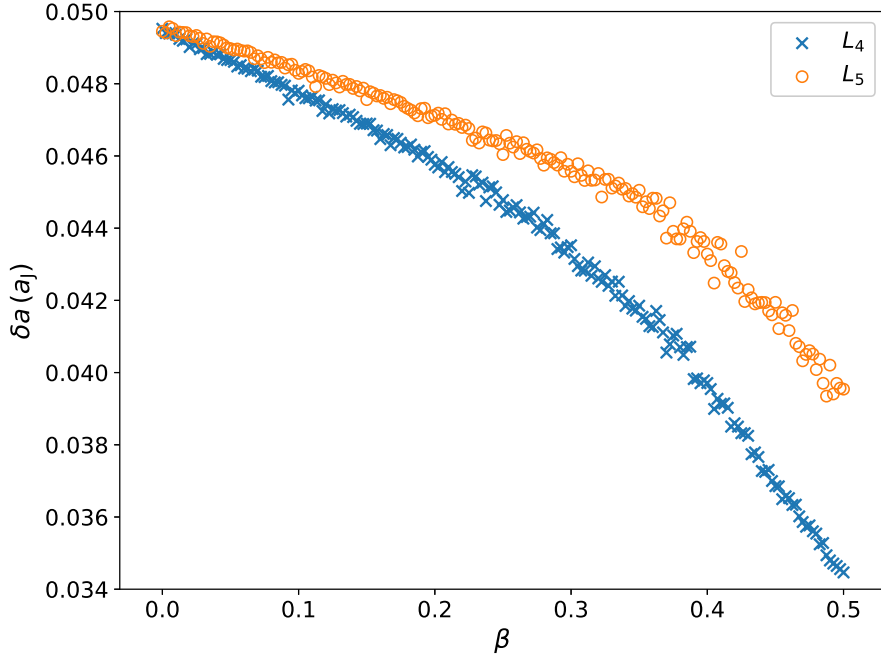


Figure 11: Dependency of the extension of the regime of librational motion δa (in units of the semi-major axis of Jupiter δ_J) on parameter β in the uncharged problem.

Poynting-Robertson effect also triggers the asymmetry between the extend of the two tadpole regimes of motion around L_4 and L_5 .

The effect of charge on the width of the librational regime of motions is clearly demonstrated in Fig. 6. However, the determination of the maximum libration amplitude is not as straightforward as in the uncharged case. The librational regime (indicated in blue) is tilted and irregular, and moreover depends quite sensitively on the integration time. For this reason we skip the study on the librational regime of motion in the charged problem and investigate the time of temporary capture instead. For this reason, we perform a series of numerical integrations for initial conditions starting at the minimum libration amplitude location close to L_4 and L_5 and keep track of the time of temporary capture in the vicinity of the 1 : 1 MMR defined by the time at which the dust grain leaves the regime of motion defined by $|a(t) - a^*| > 0.286$ AU. The choice, that corresponds to about $0.055a_J$, is made to cover the full tadpole regime of motions in the pure gravitational case (see top of Fig. 2). The results for the uncharged problem are reported in Fig. 12. Here, the capture time in mean motion resonance with Jupiter starting close to L_4 is marked by blue crosses,

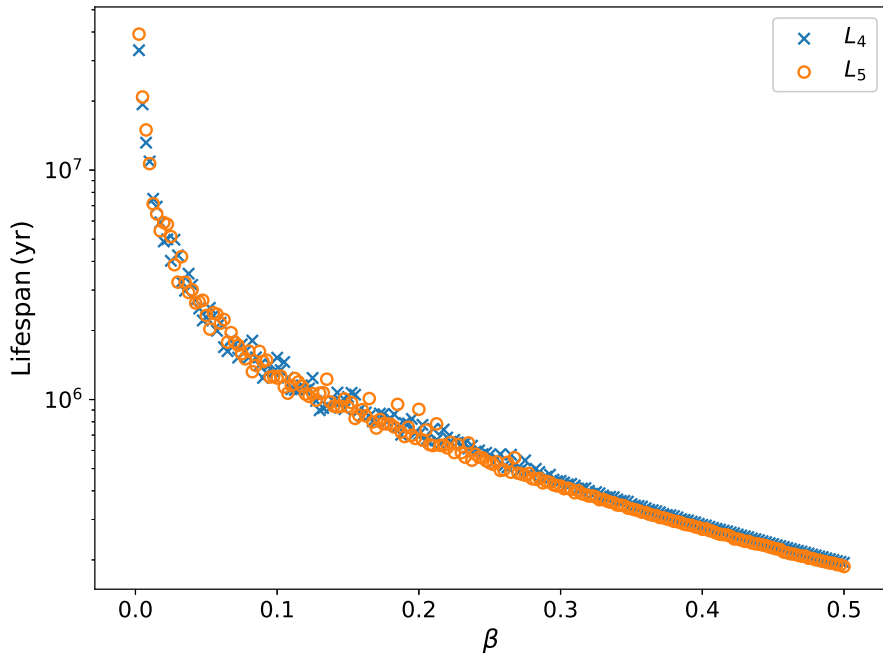


Figure 12: Dependency of the time of temporary capture in 1 : 1 MMR with planet Jupiter on parameter β in the uncharged problem.

the capture time for orbits starting in the vicinity of L_5 is shown by orange circles. Interestingly, the capture time, very close to the centers of the CRTBP, is more or less the same for both sets of initial conditions and changing β .

The results for the case $\gamma > 0$, i.e. a dust surface charge potential of 5 Volts and 10 Volts is shown in Fig. 13. For small values of β capture close to L_4 and L_5 takes place on comparable times with a slightly large lifespan for $U = 5V$ (crosses) compared to the case $U = 10V$. Beyond $\beta \simeq 0.1$ capture times behave more irregular, possibly due to the chaotic nature of the problem. However, we still see an increase in capture time for the smaller value of dust grain surface potential U (compare the location of crosses and circles in Fig. 13).

4 A simplified model for charged co-orbital motion

In this section we develop a simplified mathematical model based on the circular restricted three-body problem and including Lorentz force, and Poynting-Robertson effect. It is valid very close to exact 1:1 mean motion resonance and is accurate for small values of eccentricity e and orbital inclination i of the

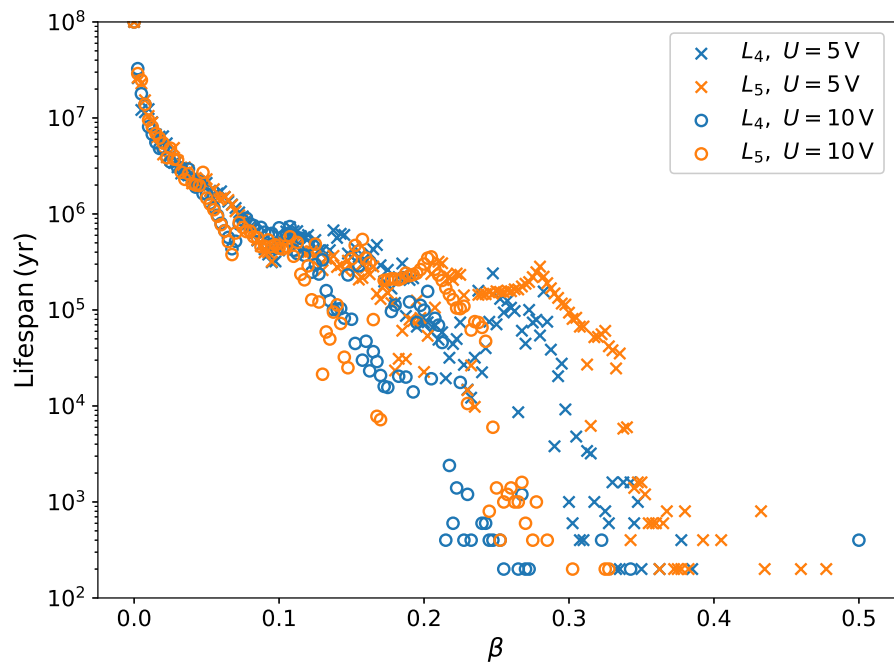


Figure 13: Dependency of the time of temporary capture in 1 : 1 MMR with planet Jupiter on parameter β in the charged problem with surface potential of 5 and 10 Volts.

charged dust particle only. The motivation of it is to understand the role of the non-gravitational effects on a , e , and i close to equilibrium values. The model is obtained using perturbation theory and averaging method in the framework of Gauss' planetary equations of motion. Our focus is on the description of the mean evolution of a , e and i during time of temporary capture on secular time scales. Let $h = \sqrt{(1-e^2)}a^2n$, $n^2a^3 = \mu$, $\theta = f + \omega$, with true anomaly f , and eccentric anomaly E . We start with the variational equations related to semi-major axis, eccentricity, and inclination [Fitzpatrick, 2012]:

$$\begin{aligned}\frac{da}{dt} &= \frac{2h(F_T(e \cos(\theta) + 1) + eF_R \sin(\theta))}{(1-e^2)\mu} \\ \frac{de}{dt} &= \frac{h(F_T(\cos(E) + \cos(\theta)) + F_R \sin(\theta))}{\mu} \\ \frac{di}{dt} &= \frac{F_N r \cos(\theta + \omega)}{h}.\end{aligned}\tag{6}$$

where F_R , F_T , F_N are the radial, tangential, and normal components of the perturbed Kepler problem. Here, the force components are defined in a coordinate system with respect to the origin located at the position of the particle and the fundamental plane of reference coinciding with its orbital plane. The radial direction is along the line connecting the sun and the particle, the tangential direction is along the velocity vector, and the normal component is orthogonal to the orbital plane. Denoting with index j the components stemming from i) a circular perturber ($j = 1$), ii) from the Poynting-Robertson effect ($j = 2$), and iii) the interaction of the charged particle with the interplanetary magnetic field ($j = 3$), these components can be split into the form:

$$\begin{aligned}F_R &= R_1 + R_2 + R_3 \\ F_T &= T_1 + T_2 + T_3 \\ F_N &= N_1 + N_2 + N_3,\end{aligned}\tag{7}$$

and the field is related to the force functions R_j , T_j , N_j by means of ²

$$\begin{aligned}R_j &= \vec{F}_j \cdot \mathbf{R}_M \cdot (\cos(\theta), \sin(\theta), 0)^T, \\ T_j &= \vec{F}_j \cdot \mathbf{R}_M \cdot (-\sin(\theta), \cos(\theta), 0)^T, \\ N_j &= \vec{F}_j \cdot \mathbf{R}_M \cdot (0, 0, 1)^T,\end{aligned}\tag{8}$$

with $j = 1, 2, 3$. Substitution of R_i , T_i , N_i separately into (6) results in the variations in orbital parameters a , e and i due to the different perturbations. The functional form of each force component in (2) depends on r , x , y , z and either on v_x , v_y , v_z (Poynting-Robertson effect, Lorentz force) or on r_1 , x_1 ,

²See definition of rotation matrix \mathbf{R}_M in (10).

y_1, z_1 (the position of the circular perturber). First, we need to express these quantities in terms of orbital elements. Assuming small values of e and i we start with the 2nd order expansions [Dvorak and Lhotka, 2013]:

$$\begin{aligned}
\frac{r}{a} &= 1 + \frac{1}{2}e^2 - 2e \sum_{\nu=1}^4 \frac{dJ_\nu(\nu e)}{de} \frac{\cos(\nu M)}{\nu^2} + O(e^3), \\
\cos(f) &= 2 \frac{1-e^2}{e} \sum_{\nu=1}^4 J_\nu(\nu e) \cos(\nu M) - e + O(e^3), \\
\sin(f) &= 2\sqrt{1-e^2} \sum_{\nu=1}^4 \frac{dJ_\nu(\nu e)}{de} \frac{\sin(\nu M)}{\nu} + O(e^3), \\
X &= 2a \sum_{\nu=1}^4 \frac{dJ_\nu(\nu e)}{de} \frac{\cos(\nu M)}{\nu^2} - \frac{3ae}{2} + O(e^3), \\
Y &= 2a \frac{\sqrt{1-e^2}}{e} \sum_{\nu=1}^4 J_\nu(\nu e) \frac{\sin(\nu M)}{\nu} + O(e^3)
\end{aligned} \tag{9}$$

(note that $Z = 0$). Here, $J_\nu = J_\nu(x)$, with integer index ν , denote the Bessel functions of the 2nd kind. The transformation from the orbital frame (X, Y, Z) to the ecliptic frame (x, y, z) is given by the rotation matrix (see Fig.1):

$$\mathbf{R}_M = \mathbf{R}_3(\Omega) \cdot \mathbf{R}_1(i) \cdot \mathbf{R}_3(\omega), \tag{10}$$

with rotation matrices $\mathbf{R}_1, \mathbf{R}_3$ and using the transformation

$$(x, y, z)^T = \mathbf{R}_M \cdot (X, Y, Z)^T. \tag{11}$$

The quantities $\dot{r}, \dot{\vec{r}}$ can be easily obtained from above relations by application of the operator d/dt and taking into account the dependency on time of mean anomaly $M = nt + M(0)$. To formulate x_1, y_1, z_1 in terms of Kepler elements, we make the assumption of a circular perturber ($e_1 = 0$) moving within the ecliptic ($i_1 = 0$), and with vanishing perihel ($\omega_1 = 0$) and longitude of the ascending node ($\Omega_1 = 0$). Denoting by a_1 the semi-major axis of the gravitational perturber, the above relations reduce to (note that $z_1 = 0$):

$$\begin{aligned}
x_1 &= a_1 \cos(M_1), \\
y_1 &= a_1 \sin(M_1),
\end{aligned} \tag{12}$$

with $M_1 = n_1 t$ and $n_1^2 a_1^3 = \mu$. For the expansion of the expression,

$$\frac{\vec{r}_1 \cdot \vec{r}}{r_1^3} - \frac{1}{\Delta} - \frac{1}{r}, \tag{13}$$

that enters the potential in (2) up to $O(e^3)$ we first approximate the term (13) close to $r/r_1 \simeq 1$, and by making use of the identity:

$$\cos(\psi) = \frac{\vec{r} \cdot \vec{r}_1}{rr_1} . \quad (14)$$

Following the steps described in full detail in Lhotka and Celletti [2015], the terms that enter (13) take the form

$$\begin{aligned} \frac{1}{\Delta} &= \frac{1}{\sqrt{2}} \frac{1}{r_1} \left(\sum_{j=0}^{\infty} (-1)^j \binom{-1/2}{j} \cos(\psi)^j \sum_{n=0}^{\infty} \binom{-1/2}{n} \epsilon^n \right) , \\ \frac{\vec{r}_1 \cdot \vec{r}}{r_1^3} &= \frac{r \cos(\psi)}{r_1^2} , \end{aligned} \quad (15)$$

with $\epsilon = r/r_1 (1 + A^{-1}r/r_1)$, and $A = 2(1 - \cos(\psi))$. In the following, we make use of these expansions truncated at $(r/r_1)^2$ and $\cos^{12} \psi$. To obtain \vec{F}_1 we require the gradients of (15) that become:

$$\frac{dr}{dx} = \frac{x}{r} , \frac{dr}{dy} = \frac{y}{r} , \frac{dr}{dz} = \frac{z}{r} ,$$

as well as

$$\frac{d \cos(\psi)}{dx} = \frac{x_1}{rr_1} , \frac{d \cos(\psi)}{dy} = \frac{y_1}{rr_1} , \frac{d \cos(\psi)}{dz} = \frac{z_1}{rr_1} .$$

Using (9) together with above expressions the vector field \vec{F}_1 is completely determined by the gradient of the potential

$$\Phi_1 = -\mu_1 \left(\frac{\vec{r}_1 \cdot \vec{r}}{r_1^3} - \frac{1}{\Delta} - \frac{1}{r} \right) , \quad (16)$$

We insert (7), (8) in (6) using (9) - (16), and $\vec{F}_1 = -\nabla \Phi_1$, and only retain trigonometric terms in the expansions of (6) that are of the form:

$$k(M + \omega + \Omega - M_1) + l\omega + m\Omega ,$$

with $(k, l, m) \in \mathbb{Z}^3$. The resulting vector field only contains resonant terms that are trigonometric in resonant argument $\sigma = \lambda - \lambda_1$, with $\lambda = M + \omega + \Omega$, and without explicit dependence on the orbital longitude of the perturber $\lambda_1 = M_1$. Let superscript ⁽¹⁾ label the orbital variation due to the perturber. To 2nd order in r/r_1 , 12th order in $\cos(\psi)$ and 2nd order in e we obtain the system:

$$\begin{aligned}
\frac{da^{(1)}}{dt} &= \sum_{k,l,m} c_{k,l,m}^{(a)}(e) \cos(ki) \sin(l\sigma + m\omega) , \\
\frac{de^{(1)}}{dt} &= \sum_{k,l,m} c_{k,l,m}^{(e)}(e) \cos(ki) \sin(l\sigma + m\omega) , \\
\frac{di^{(1)}}{dt} &= \sum_{k,l,m} c_{k,l,m}^{(i)}(e) \sin(ki) \sin(l\sigma + m\omega) , \tag{17}
\end{aligned}$$

with $k, l = 1, \dots, 12$, $m = -4, -2, 0, 2, 4$, and $c_{k,l,m}^{(a,e,i)}$ polynomial in eccentricity e . We notice that the vector field does not explicitly depend on ascending node longitude Ω . From standard theory of the circular restricted three-body problem we know [Dvorak and Lhotka, 2013] that the reference solution for the stable equilibria L_4, L_5 is given by $a_* = a_J$, $e_* = e_J = 0$, $i_* = i_J = 0$, $\omega_* = \omega_J = 0$, $\Omega_* = \Omega_J = 0$, and $M_* = M_J \pm 60^\circ$. The solution defined by the pure gravitational problem from (17) is determined by the condition:

$$\frac{da^{(1)}}{dt} = \frac{de^{(1)}}{dt} = \frac{di^{(1)}}{dt} = 0 . \tag{18}$$

To solve this system we substitute $M_* = \pm 60^\circ$, and $\omega_* = \Omega_* = 0$ and solve for the remaining $a_*^{(1)}$, $e_*^{(1)}$, $i_*^{(1)}$ using a numerical scheme (Newton method). A comparison with the reference solution provides an estimate of the error in the approximation of the exact problem.

4.1 The role of radiative effects on shift in a

The shift due to parameter β that enters \vec{F}_0 in (1) has been found to follow $a = a_J (1 - \beta)^{1/3}$, the shift in σ is given in the upper plot of Fig. 5, obtained numerically, and on the basis of a simplified formula in synodic coordinates [Zhou et al., 2021].

To estimate the role of the combined PR and solar wind effect on the Kepler elements we make use of Eq.(14) in Lhotka and Celletti [2015], where the secular effect on semi-major axis a and eccentricity e is simply given by:

$$\begin{aligned}
\frac{da^{(2)}}{dt} &= -\frac{a(1 + 3e^2)\mu\beta n}{c(1 - e^2)^{3/2}} , \\
\frac{de^{(2)}}{dt} &= -\frac{\mu\beta n}{\sqrt{aec}} \left(\frac{(3 + 2e)e}{2\sqrt{1 - e^2}} \right) , \tag{19}
\end{aligned}$$

and $di^{(2)}/dt = 0$ (supscript ⁽²⁾ indicates again the link of (19) with \vec{F}_2). We notice that radiative effects do not affect the orbital planes, and the signs that enter in front of (19) indicate that the orbits of the dust particles are shrinking in a and circularizing in e with time. Taking $n = \sqrt{\mu/a^3}$ and then $a =$

$a_J(1 - \beta)^{1/3}$ a Taylor series expansion with respect to β gives to zeroth order in e the estimate:

$$\frac{da^{(2)}}{dt} \simeq -\frac{\mu^{3/2}}{\sqrt{a_J}c} \left(\beta + \frac{\beta^2}{6} \dots \right) \lesssim 1.9 \times 10^{-5} \beta ,$$

and $de^{(2)}/dt \simeq 0$, where we substituted for the parameters μ, a_J, c to obtain the inequality. The magnitudes being small, the shift of the equilibrium values in a and e can be neglected in comparison to the shift $a_J(1 - \beta)^{1/3}$. However, the effect is sufficient to render the equilibria unstable, and are therefore responsible for the phenomenon of temporary capture close to L_4 and L_5 , respectively [see, e.g. Murray, 1994, Lhotka and Celletti, 2015].

4.2 The role of the interplanetary magnetic field on i

To model the mean effect on a, e, i that is stemming from the interaction of the charged dust particle with the interplanetary magnetic field, i.e. \vec{F}_3 in (1), we proceed as follows. Assuming a standard Parker spiral model [Lhotka and Narita, 2019] of the mean magnetic field we make use of the expressions developed in Lhotka and Galeş [2019], i.e. Eq. (24):

$$\frac{di^{(3)}}{dt} = -\alpha \frac{q}{m} \frac{B_0}{2} \left(\frac{r_0}{a} \right)^2 \left\{ \left[1 - \cos(i) z_0 \frac{\Omega_s}{n} \right] \times \left(x_0 \cos(\Omega) + y_0 \sin(\Omega) \right) \right\} . \quad (20)$$

Here, $x_0 = \sin(\Omega_0) \sin(i_0)$, $y_0 = -\sin(i_0) \cos(\Omega_0)$, $z_0 = \cos(i_0)$, that locate the magnetic dipole axis of the rotating sun in the inertial reference frame, see Fig. 1. We notice that (20) is valid for small x_0, y_0 , and $1 - z_0$ and vanishing eccentricity only. Moreover, we essentially neglect the influence of the radial and tangent components F_R, F_T in (6), that have been shown to vanish over one revolution period of the dust particle [Lhotka and Galeş, 2019]. However, we stress that the modification of the standard Parker spiral model to include a magnetic field normal component B_N will result in secular evolution of da/dt , de/dt , and di/dt [see, Eq. (14) in Lhotka et al., 2016]. Since we assume $B_N = 0$ throughout the paper we may use (20) to investigate the role of Lorentz force on the orbital evolution of inclination of the dust particles.

From numerical studies in Sec. 3 we already found that the inclusion of the interplanetary magnetic field on the dynamics triggers periodic variations of the orbital planes of the charged dust particles as shown on the lower left in Fig. 4. Following the approach developed in Lhotka and Galeş [2019] we estimate the net effect on the orbital inclination as follows. From the condition $x_0 \cos(\Omega) + y_0 \sin(\Omega) = 0$ we find $\Omega = \Omega_0$ and as a consequence $di/dt = 0$ in (20). The turning points in i should therefore take place whenever the line of nodes related to ascending node longitudes coincide with the line of nodes formed between the equatorial and ecliptic planes located at angular distance $\Omega = \Omega_0 = 73.5^\circ$. The result is visualized in Fig.14 for a test particle starting with $i(0) = 10^\circ$. At the beginning the inclination of the charged dust particle

increases. After a period of time of about $100y$ the ascending node of the dust particle crosses $\Omega = \Omega_0 = 73.5^\circ$, where we have $di/dt = 0$ and the maximum excursion in $i = i_{max} \simeq 18^\circ$. The effect of Lorentz force reverses, and inclination decreases until the minimum $i_{min} \simeq 3^\circ$ is reached at time $t \simeq 260y$, where ascending node longitude passes $\Omega = \Omega_0 + 180^\circ$, and inclination starts to rise again. The simple analysis on the basis of (20) provides libration amplitudes in inclination i of about 15° with libration period of about $320y$ which is consistent with numerical simulations.

5 Summary & Conclusions

In this work we study the dynamics of charged dust close to the Lagrangian points L_4 and L_5 and subject to solar wind, Poynting-Robertson (PR) effect, and the interplanetary magnetic field, with special focus on the Lorentz force term. We provide the shift and extent of the tadpole regime of motions in dependency on the system parameters, i.e. the charge-to-mass ratio γ of the dust grains. We quantify the asymmetry between the location and size of librational kind of motions between L_4 and L_5 which is mainly due to radiative effects and the Lorentz force term. The shift in resonant argument σ due to the solar wind and the PR-effect from the pure gravitational solution $\sigma = \pm 60^\circ$ is larger with respect to L_4 in comparison with L_5 . For small charge-to-mass ratios the shift due to Lorentz force is small, but may increase to several degrees with decreasing radius R of the charged dust grain. A similar behaviour can be found in the angular separation $\Delta\omega = \omega - \omega_J$ from the value $\pm 60^\circ$ of the pure gravitational, elliptic problem. The displacement in semi-major axis a from a_J of Jupiter is dominated by solar radiation pressure, following $a \simeq (1 - \beta)^{(1/3)}a_J$, with increasing ratio β between solar radiation over pure gravitational attraction. However, it is found that Lorentz force may contribute to this displacement with increasing values of γ . One important finding of our study is the role of γ on $\Delta e = e - e_J$ that vanishes at the Lagrange points of the pure gravitational problem. While radiation pressure, solar wind, and the PR-effect leads to marginal variations in Δe , Lorentz force may trigger large deviations from zero at the minimum libration amplitude solutions. Another important phenomenon that can only be explained by the Lorentz force, i.e. the interaction of the charged dust grains with the interplanetary magnetic field, are periodic variations on secular time scales in inclination i and ascending node longitude Ω . Using a simplified model on the basis of Gauss averaged equations of motion, conditions for maxima and minima of these excursions in inclinations can be found with libration amplitudes up to several degrees. We also observe amplitude enhancements in the orbital evolution of the resonant argument σ whenever the periods of ascending node longitude Ω and σ coincide. Since the period in Ω depends on the actual charge-to-mass ratio γ the phenomenon occurs at specific values of γ only. Last, but not least we perform a series of simulations to estimate the time of temporary capture of charged dust close to the 1:1 mean motion resonance with planet Jupiter, and find a decrease in

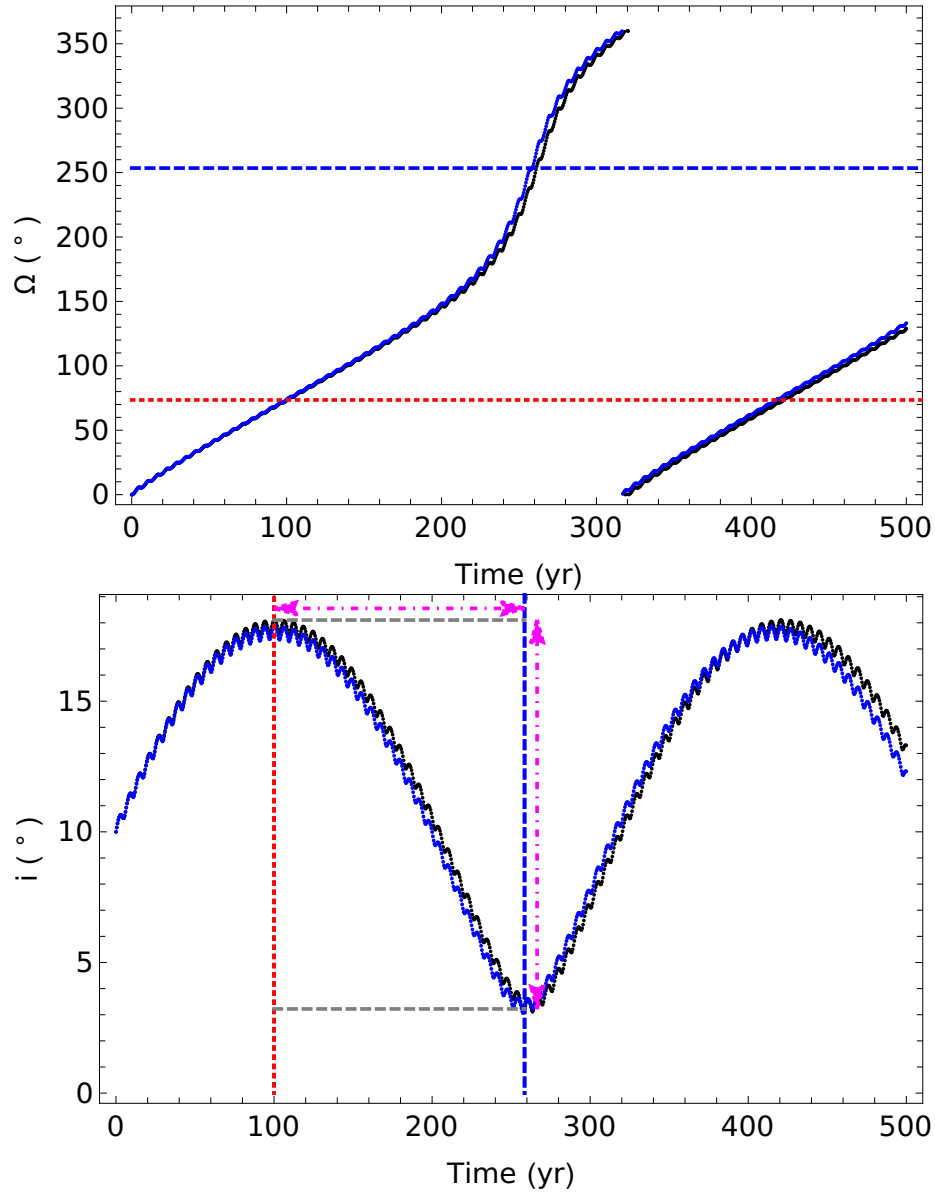


Figure 14: Timeseries for ascending node longitude Ω (top) and inclination (bottom) for a dust particle of radius $R = 2.05\mu m$ with $4.43V$ surface charge, starting at $a(0) = a_J$, $e = 0.01$, $i(0) = 10^\circ$. Red-dotted lines mark $\Omega = \Omega_0 = 73.5^\circ$ where $i = i_{max}$, blue-dashed lines $\Omega = \Omega_0 + 180 = 253.5^\circ$, where $i = i_{min}$. Arrows (dot-dashed magenta) indicate $i_{max} - i_{min} \simeq 15^\circ$, and the timespan between maxima and minima (about 160 years).

capture time for charged dust in comparison to neutral one. We notice that our model of the interplanetary magnetic field is very simple, i.e. it does not include time dependent effects stemming from the activity of the Sun. Our results are therefore not suitable to interpret observations. However, even this simple model already shows the important role of the solar wind, together with the interplanetary magnetic field on resonant kind of motions of charged dust in planetary systems. More realistic models of the interplanetary magnetic field, and time dependent effects will be subject to future studies in the field.

Acknowledgements This work is funded by the Austrian Science Fund (FWF) within the project P-30542 entitled 'Stability of charge and orbit of cosmic dust particles'. CL acknowledges the support of EU H2020 MSCA ETN Stardust-Reloaded Grant Agreement 813644, MIUR Excellence Department Project awarded to the Department of Mathematics, University of Rome Tor Vergata, CUP E83C18000100006, MIUR-PRIN 20178CJA2B 'New Frontiers of Celestial Mechanics: theory and Applications', and GNFM/INdAM. LZ acknowledges the support of China Scholarship Council (No. 201906190106), National Natural Science Foundation of China (NSFC, Grants No. 11473016, No. 11933001), and National Key R&D Program of China (2019YFA0706601).

The authors declare that they have no conflict of interest.

References

- E.M. Alessi, C. Colombo, and A. Rossi. Phase space description of the dynamics due to the coupled effect of the planetary oblateness and the solar radiation pressure perturbations. *Celestial Mechanics and Dynamical Astronomy*, 131(9):43, September 2019. doi: 10.1007/s10569-019-9919-z.
- C. Beauge and S. Ferraz-Mello. Capture in exterior mean-motion resonances due to Poynting-Robertson drag. *Icarus*, 110:239–260, August 1994. doi: 10.1006/icar.1994.1119.
- J. G. Beck and P. Giles. Helioseismic Determination of the Solar Rotation Axis. *ApJ Letters*, 621:L153–L156, March 2005. doi: 10.1086/429224.
- A. Celletti, C. Gales, and C. Lhotka. (INVITED) Resonances in the Earth's space environment. *Communications in Nonlinear Science and Numerical Simulations*, 84:105185, May 2020. doi: 10.1016/j.cnsns.2020.105185.
- R. Dvorak and C. Lhotka. *Celestial Dynamics*. John Wiley & Sons, Ltd , 2013.
- J. Feng and X. Y. Hou. Secular dynamics around small bodies with solar radiation pressure. *Communications in Nonlinear Science and Numerical Simulations*, 76:71–91, September 2019. doi: 10.1016/j.cnsns.2019.02.011.
- R. Fitzpatrick. *An Introduction to Celestial Mechanics*. UK Cambridge University Press, September 2012.

- E. Grün, H. A. Zook, M. Baguhl, A. Balogh, S. J. Bame, H. Fechtig, R. Forsyth, M. S. Hanner, M. Horanyi, J. Kissel, B. A. Lindblad, D. Linkert, G. Linkert, I. Mann, J. A. M. McDonnell, G. E. Morfill, J. L. Phillips, C. Polanskey, G. Schwehm, N. Siddique, P. Staubach, J. Svestka, and A. Taylor. Discovery of Jovian dust streams and interstellar grains by the Ulysses spacecraft. *Nature*, 362(6419):428–430, April 1993. doi: 10.1038/362428a0.
- J. Klačka. Solar wind dominance over the Poynting-Robertson effect in secular orbital evolution of dust particles. *MNRAS*, 443:213–229, September 2014. doi: 10.1093/mnras/stu1133.
- J. Klačka, J. Petržala, P. Pástor, and L. Kómar. Solar wind and the motion of dust grains. *Monthly Notices Royal Astronomical Society*, 421(2):943–959, April 2012. doi: 10.1111/j.1365-2966.2012.20321.x.
- D. Koschny, R. H. Soja, C. Engrand, G. J. Flynn, J. Lasue, A.-C. Levasseur-Regourd, D. Malaspina, T. Nakamura, A. R. Poppe, V. J. Sterken, and J. M. Trigo-Rodríguez. Interplanetary Dust, Meteoroids, Meteors and Meteorites. *Space Science Reviews*, 215(4):34, June 2019. doi: 10.1007/s11214-019-0597-7.
- H. Krüger, P. Strub, N. Altobelli, V. J. Sterken, R. Srama, and E. Grün. Interstellar dust in the solar system: model versus in situ spacecraft data. *A&A*, 626:A37, June 2019. doi: 10.1051/0004-6361/201834316.
- C. Lhotka and A. Celletti. The effect of Poynting-Robertson drag on the triangular Lagrangian points. *Icarus*, 250:249–261, April 2015. doi: 10.1016/j.icarus.2014.11.039.
- C. Lhotka and C. Galeş. Charged dust close to outer mean-motion resonances in the heliosphere. *Celestial Mechanics and Dynamical Astronomy*, 131(11):49, November 2019. doi: 10.1007/s10569-019-9928-y.
- C. Lhotka and Y. Narita. Kinematic models of the interplanetary magnetic field. *Annales Geophysicae*, 37(3):299–314, May 2019. doi: 10.5194/angeo-37-299-2019.
- C. Lhotka, P. Bourdin, and Y. Narita. Charged Dust Grain Dynamics Subject to Solar Wind, Poynting-Robertson Drag, and the Interplanetary Magnetic Field. *Astrophysical Journal*, 828:10, September 2016. doi: 10.3847/0004-637X/828/1/10.
- C. Lhotka, N. Rubab, O. W. Roberts, J. C. Holmes, K. Torkar, and R. Nakamura. Charging time scales and magnitudes of dust and spacecraft potentials in space plasma scenarios. *Physics of Plasmas*, 27(10):103704, October 2020. doi: 10.1063/5.0018170.
- X. Liu and J. Schmidt. Dust arcs in the region of Jupiter’s Trojan asteroids. *A&A*, 609:A57, January 2018a. doi: 10.1051/0004-6361/201730951.

- X. Liu and J. Schmidt. Comparison of the orbital properties of Jupiter Trojan asteroids and Trojan dust. *A&A*, 614:A97, June 2018b. doi: 10.1051/0004-6361/201832806.
- I. Mann, N. Meyer-Vernet, and A. Czechowski. Dust in the planetary system: Dust interactions in space plasmas of the solar system. *Physics Reports*, 536(1):1–39, March 2014. doi: 10.1016/j.physrep.2013.11.001.
- A. Margheri and M. Misquero. A dissipative Kepler problem with a family of singular drags. *Celestial Mechanics and Dynamical Astronomy*, 132(3):17, March 2020. doi: 10.1007/s10569-020-9956-7.
- N. Meyer-Vernet. *Basics of the Solar Wind*. Cambridge University Press, 2012, September 2012.
- M. Moretto and J. McMahon. Evolution of orbits about comets with arbitrary comae. *Celestial Mechanics and Dynamical Astronomy*, 132(6-7):37, July 2020. doi: 10.1007/s10569-020-09973-5.
- C. D. Murray. Dynamical Effects of Drag in the Circular Restricted Three-Body Problem. I. Location and Stability of the Lagrangian Equilibrium Points. *Icarus*, 112(2):465–484, December 1994. doi: 10.1006/icar.1994.1198.
- P. Pokorný and M. Kuchner. Co-orbital Asteroids as the Source of Venus’s Zodiacal Dust Ring. *Astrophysical Research Letters*, 873(2):L16, March 2019. doi: 10.3847/2041-8213/ab0827.
- A. R. Poppe. An improved model for interplanetary dust fluxes in the outer Solar System. *Icarus*, 264:369–386, January 2016. doi: 10.1016/j.icarus.2015.10.001.
- A. R. Poppe. The contribution of Centaur-emitted dust to the interplanetary dust distribution. *MNRAS*, 490(2):2421–2429, December 2019. doi: 10.1093/mnras/stz2800.
- A. R. Poppe and C. O. Lee. The Effects of Solar Wind Structure on Nanodust Dynamics in the Inner Heliosphere. *Journal of Geophysical Research (Space Physics)*, 125(10):e28463, October 2020. doi: 10.1029/2020JA028463.
- D. W. Schuerman. The restricted three-body problem including radiation pressure. *The Astrophysical Journal*, 238:337–342, May 1980. doi: 10.1086/157989.
- Frank Spahn, Manuel Sachse, Martin Seiß, Hsiang-Wen Hsu, Sascha Kempf, and Mihály Horányi. Circumplanetary Dust Populations. *Space Science Reviews*, 215(1):11, January 2019. doi: 10.1007/s11214-018-0577-3.
- L. Zhou, C. Lhotka, C. Gales, Y. Narita, and L.-Y. Zhou. Dynamics of charged dust in the orbit of Venus. *A&A*, 645:A63, January 2021. doi: 10.1051/0004-6361/202039617.